An Oligomer Study on Small Band Gap Polymers

Bram P. Karsten,[†] Lucas Viani,[‡] Johannes Gierschner,[‡,§] Jérôme Cornil,[‡] and René A. J. Janssen*,[†]

Laboratory of Macromolecular and Organic Chemistry, Eindhoven University of Technology, P.O. Box 513, NL-5600 MB Eindhoven, The Netherlands, Laboratory for Chemistry of Novel Materials, University of Mons-Hainaut, Place du Parc 20, B-7000 Mons, Belgium, and Madrid Institute for Advanced Studies, IMDEA-Nanoscience, Madrid, Spain

Received: July 2, 2008; Revised Manuscript Received: August 24, 2008

Small band gap polymers may increase the energy conversion efficiency of polymer solar cells by increased absorption of sunlight. Here we present a combined experimental and theoretical study on the optical and electrochemical properties of a series of well-defined, lengthy, small band gap oligo(5,7-bis(thiophen-2-yl)thieno[3,4-b]pyrazine)s ($E_g = 1.50$ eV) having alternating donor and acceptor units. The optical absorptions of the ground state, triplet excited state, radical cation, and dication are identified and found to shift to lower energy with increasing chain length. The reduction of the band gap in these alternating small band gap oligomers mainly results from an increase of the highest occupied molecular orbital (HOMO) level. The S_1-T_1 singlet−triplet splitting is reduced from ∼0.9 eV from the trimeric monomer to –0.5 eV for the pentamer. This significant exchange energy is consistent with the fact that both the HOMO and the lowest unoccupied molecular orbital (LUMO) remain distributed over virtually all units, rather than being localized on the D and A units.

Introduction

Polymer solar cells are an attractive means for converting sunlight directly into electricity. Because of their flexibility, ease of processing, and their potential low cost manufacture, polymer solar cells could be serious candidates for replacing current energy resources. In recent years, tremendous advances have been made in increasing the efficiency of solar cells containing polymers such as polythiophene.[1−3] The photocurrent in these devices is, however, limited by the poor overlap between the spectrum of the sun and the absorption spectrum of the polymer.[4] This poor spectral overlap results in the loss of a large fraction of the energy contained in the sunlight, because photons with energies below ca. 2 eV are not absorbed. This is by far the largest fraction of the light emitted by the sun.

To increase spectral overlap, reduction of the band gap of π-conjugated polymers is necessary. Hence, high-efficiency organic solar cells will consist, at least partially, of small band gap polymers. To date, several conjugated polymers with reduced band gaps have been reported,[5−15] yielding energy conversion efficiencies up to 5.5% under simulated solar light.[15] The way generally taken to reduce the band gaps of conjugated polymers is to incorporate segments with alternating electron-rich donor and electron-deficient acceptor units in the polymer backbone.[16,17] As donor segments, generally thiophene units, or derivatives, have been employed. Acceptor units can vary, e.g., benzothiadiazole,[8,11] thienopyrazine,[7,9,10] and related compounds have been found to be useful.

As the field of small band gap polymers is rapidly expanding, it is important to investigate the detailed electro-optical properties of these systems and understand how these characteristics can evolve with chain length. To date, experimental studies on small band gap oligomers have been restricted to short-chain oligomers;[18] extended systems have been studied by quantum-chemical methods.[19,20] Knowledge about the electrochemical and optical properties of oligomers of small band gap systems will help in gaining valuable insight into the design rules for new materials and into the processes limiting the efficiency of polymer solar cells. Knowledge of the chain-length dependence of, e.g., band gap, highest occupied molecular orbital (HOMO) and lowest unoccupied molecular orbital (LUMO) levels, and triplet energies can help with the design of new polymers with optimized properties for solar energy conversion.

In this work, we present a combined experimental and theoretical study on the properties of small band gap oligomers that comprise electron-rich thiophene units alternating with an electron-deficient thienopyrazine, similar to materials recently described for solar cells.[10] Oligomers were synthesized by polymerizing the monomer in the presence of a chain stopper, yielding a mixture of short oligomers. The oligomers produced in this way could be efficiently separated by recycling gel permeation chromatography (GPC). Subsequently, the chain length dependence of the absorption spectra, oxidation and reduction potentials, triplet levels, triplet absorptions, and the properties of the oxidized species were investigated. The electronic and optical properties of the neutral oligomers were estimated at a quantum-chemical level.

Experimental Methods

General Methods. ^{1}H NMR and ^{13}C NMR spectra were recorded on a 400 MHz NMR (Varian Mercury, 400 MHz for ^{1}H NMR and 100 MHz for ^{13}C NMR), and chemical shifts are reported in parts per million (ppm) downfield from tetramethylsilane (TMS). IR spectra were recorded on a Perkin-Elmer 1600 Fourier transform infrared (FT-IR) spectrometer. Matrix-assisted laser desorption ionization time-of-flight (MALDI-TOF) mass spectrometry was performed on a PerSeptive Biosystems

* Corresponding author. E-mail: r.a.j.janssen@tue.nl.
† Eindhoven University of Technology.
‡ University of Mons-Hainaut.
§ Madrid Institute for Advanced Studies.

10.1021/jp805817c CCC: $40.75
Published on Web 10/01/2008

Voyager-DE PRO spectrometer. UV/vis spectra were recorded on a Perkin-Elmer Lambda 900 UV/vis/NIR spectrometer. GPC analysis of the oligomers was performed on a liquid chromatography (LC) system, equipped with two PLgel 3 μm 100 Å GPC columns and a photodiode array detector. The eluent was chloroform, using a flow of 1 mL/min and an injection volume of 20 μL. GPC analysis of the polymer was performed at 80 °C on an LC system equipped with a PLgel 5 μm Mixed_C column and UV and refractive index detectors. The eluent was *o*-dichlorobenzene (ODCB), using a flow of 1 mL/min and an injection volume of 20 μL. Recycling GPC was performed on a LC system equipped with JAIGEL 2H and JAIGEL 2.5H columns and a UV-detector set at 400 and 600 nm, using a preparative flow cell (path length 0.5 mm). The eluent was chloroform at 3.5 mL/min, and the injection volume was 2 mL. Cyclic voltammograms were recorded in an inert atmosphere with 0.1 M tetrabutyl ammonium hexafluorophosphate ($TBAPF_6$) in ODCB as the supporting electrolyte. The working electrode was a platinum disk (0.2 cm^2), and the counter electrode was a platinum electrode. Three different scan speeds were used for all compounds (50, 100, and 200 mV/s). The samples were measured using a Ag/AgCl reference electrode with Fc/Fc^+ as an internal standard using a μAutolab II with a PGSTAT30 potentiostat. Photoinduced absorption (PIA) spectra were recorded by exciting with a mechanically modulated continuous-wave (cw) Ar-ion laser (λ = 351 and 364 nm, 275 Hz) pump beam and monitoring the resulting change in the transmission of a tungsten-halogen probe light through the sample (ΔT) with a phase-sensitive lock-in amplifier after dispersion by a grating monochromator and detection, using Si, InGaAs, and cooled InSb detectors. The pump power incident on the sample was typically 25 mW with a beam diameter of 2 mm. The PIA ($\Delta T/T$) was corrected for the photoluminescence, which was recorded in a separate experiment. PIA spectra and photoluminescence spectra were recorded with the pump beam in a direction almost parallel to the direction of the probe beam. The solutions were studied in a 1 mm near-IR grade quartz cell at room temperature, except for the polymer, which was studied at 80 °C.

Materials. Solvents were purchased from Biosolve and used without further purification, unless stated otherwise, tetrahydrofuran (THF) was distilled over 4 Å molsieves before use. Chemicals were purchased from Acros or Aldrich and used without purification. *N*-bromosuccinimide (NBS) was recrystallized from water. 3,3″-Dioctyl-[2,2′;5′,2″]terthiophene-3′,4′-diamine (**1**) was prepared according to a literature procedure.[7] Biobeads S-X1 were obtained from Bio-Rad Laboratories. Oxygen and moisture-sensitive reactions were performed under an argon atmosphere.

5,10-Diethyl-tetradecane-7,8-dione (2). 2-Ethylhexyl bromide (9 mL, 50 mmol) was added dropwise to iodine-activated magnesium (1.28 g, 52.5 mmol) in THF (40 mL). The mixture was stirred for 1 h at reflux. A solution of LiBr (8.7 g, 100 mmol) in THF (40 mL) was added at room temperature to a stirred suspension of CuBr (7.2 g, 50 mmol) in THF (40 mL). Grignard solution was added dropwise, via a syringe, at −78 °C, and the mixture was stirred at that temperature for 0.5 h. Oxalyl chloride (1.8 mL, 20 mmol) was added dropwise, and the mixture was stirred at −78 °C for 1 h. The mixture was allowed to warm to room temperature, stirred for another 0.5 h, and quenched with saturated NH_4Cl (200 mL). The product was extracted with ethyl acetate (3 × 80 mL), the organic phase was dried with $MgSO_4$, and the solvent was evaporated. The crude product was purified by column chromatography on silica (95/5 heptane/ethyl acetate), and the pure product eluted as the first band and was obtained as a yellow liquid. Yield: 2.4 g (44%). ^{1}H NMR (400 MHz) δ (ppm): 2.65 (d, J = 6.6 Hz, 4p, (CO)CH_2CH(C_4H_9)(C_2H_5)), 1.86 (m, 2p, (CO)CH_2CH(C_4H_9)(C_2H_5)), 1.45−1.10 (m, 16p, −CH_2−), 0.95−0.75 (m, 12p, −CH_3). IR (cm^{-1}): 2959, 2926, 2860, 1710, 1460, 1380.

2,3-Bis(2′-ethylhexyl)-5,7-bis(3-octylthiophen-2-yl)thieno[3,4-b]pyrazine (3). Compounds **1** (1.1 g, 2.1 mmol) and **2** (0.7 g, 2.3 mmol) were dissolved in ethanol (25 mL) and stirred at reflux for 22 h. The solvent was evaporated, and the crude product was purified by column chromatography on silica (75/35 heptane/dichloromethane). The product was isolated as a dark red oil. Yield: 1.31 g (78%). ^{1}H NMR (400 MHz) δ (ppm): 7.35 (d, J = 5.2 Hz, 2p, Ar−H), 7.00 (d, J = 5.3 Hz, 2p, Ar−H), 2.95 (t, J = 7.9 Hz, 4p, −C$H_2C_7H_{15}$), 2.84 (d, J = 6.9 Hz, 4p, −CH_2CH(C_4H_9)(C_2H_5)), 2.20 (m, 2p, −CH_2CH(C_4H_9)(C_2H_5)), 1.72 (qu, J = 7.7 Hz, 4p, −CH_2C$H_2C_6H_{13}$), 1.50−1.20 (m, 36p, −CH_2−), 0.96−0.83 (m, 18p, −CH_3). ^{13}C NMR (100 MHz) δ (ppm): 155.65, 140.24, 137.77, 129.27, 128.32, 126.19, 123.70, 39.48, 37.68, 32.85, 31.89, 30.38, 30.36, 29.78, 29.54, 29.32, 28.94, 25.93, 23.14, 22.67, 14.16, 14.08, 10.89. IR (cm^{-1}): 2956, 2924, 2855, 1463, 1378. MALDI-TOF-MS *m*/*z* (intensity, %): 748.38 (100), 749.38 (70), 750.37 (50), 751.37, 752.38.

Part of the product was further purified for characterization by column chromatography on biobeads S-X1 using chloroform as the eluent.

Monobromo and Dibromo 2,3-bis(2′-ethylhexyl)-5,7-bis-(3-octythiophen-2-yl)-thieno[3,4-b]pyrazine (4, 5). Compound **3** (433 mg, 0.58 mmol) was dissolved in THF (25 mL). NBS (166 mg, 0.93 mmol) was added at 0 °C, in the absence of light. The mixture was stirred overnight, while warming to room temperature. Diethyl ether (100 mL) was added, and the mixture was washed with water (3 × 40 mL) and saturated NaCl (2 × 40 mL). The organic phase was dried with $MgSO_4$, and the solvent was evaporated. The crude product contained a mixture of mono- and dibrominated compounds. The compounds were separated by column chromatography on silica (90/10 heptane/dichloromethane). Two fractions were collected: the first fraction contained dibrominated product (**5**) (305 mg, 58%), and the second fraction contained monobrominated product (**4**) (122 mg, 25%).

***Compound* 4.** ^{1}H NMR (400 MHz) δ (ppm): 7.3.6(d, J = 5.2 Hz, 1p, Ar−H), 7.00 (d, J = 5.2 Hz, 1p, Ar−H), 6.94 (s, 1p, ArBr−H), 2.96−2.82 (m, 8p, Ar−CH_2−), 2.20 (m, 2p, −CH_2CH(C_4H_9)(C_2H_5)), 1.76−1.66 (m, 4p, −$CH_2CH_2C_6H_{13}$), 1.55−1.18 (m, 36p, −CH_2−), 0.98−0.83 (m, 18p, −CH_3). ^{13}C NMR (100 MHz) δ (ppm): 155.94, 155.78, 140.45, 139.97, 131.73, 130.23, 129.33, 126.45, 113.55, 39.43, 37.90, 37.67, 37.52, 32.85, 32.76, 31.89, 30.55, 30.37, 30.04, 29.78, 29.71, 29.53, 29.50, 29.32, 29.28, 28.93, 25.94, 23.13, 22.65, 14.20, 14.15, 14.08, 10.93, 10.89. IR (cm^{-1}): 2956, 2923, 2854, 1638, 1521, 1460, 1407, 1378. MALDI-TOF-MS *m*/*z* (intensity, %): 826.45 (80), 827.45 (45), 828.45 (100), 829.45 (100), 830.45, 831.45.

***Compound* 5.** ^{1}H NMR (400 MHz) δ (ppm): 6.93 (s, 2p, Ar−H), 2.91−2.82 (m, 8p, Ar−CH_2−), 2.20 (m, 2p, −CH_2-CH(C_4H_9)(C_2H_5)), 1.70 (m, 4p, −CH_2C$H_2C_6H_{13}$), 1.52−1.20 (m, 36p, −CH_2−), 0.98−0.84 (m, 18p, −CH_3). ^{13}C NMR (100 MHz) δ (ppm):156.04, 140.20, 137.42, 131.77, 130.00, 122.85, 113.88, 39.39, 37.53, 32.78, 31.90, 30.60, 30.01, 29.73, 29.52, 29.30, 28.91, 25.92, 23.14, 22.67, 14.20, 14.09, 10.94. IR (cm^{-1}): 2956, 2923, 2854, 1460, 1427, 1378, 827. MALDI-TOF-MS *m*/*z* (intensity, %): 904 (50), 905 (30), 906.27 (100), 907.27 (55), 908.27 (60), 909.27 (35), 910.26.

Poly(2,3-bis(2′-ethylhexyl)-5,7-bis(3-octylthiophen-2-yl)thieno[3,4-b]pyrazine) (6). Bis(1,5-cyclooctadiene)nickel(0) (Ni(COD)$_2$) (91 mg, 0.33 mmol) and 2,2′-bipyridyl (53 mg, 0.33 mmol) were dissolved in dry and oxygen-free toluene (2 mL) and heated to 80 °C. Compound **5** (93 mg, 0.10 mmol) was added, and the mixture was stirred for 22 h at 80 °C. A 1:1:1 methanol/acetone/0.1 M HCl mixture (35 mL) was added, and the mixture was stirred for 6 h. The product was extracted with chloroform (2 × 35 mL), EDTA (disodium salt) (0.5 g) was added, and the mixture was stirred overnight. The mixture was washed with water (3 × 75 mL), concentrated, and precipitated in methanol (200 mL). The crude polymer was filtered into a Soxhlet thimble and fractionated by Soxhlet extraction with methanol, hexane, dichloromethane, chloroform, and ODCB. Yield (ODCB-fraction): 32 mg (42%). ^{1}H NMR (400 MHz) δ (ppm): 7.15 (Ar−*H*), 2.93 (Ar−C*H*$_2$−), 2.36 (−CH$_2$C*H*(C$_4$H$_9$)(C$_2$H$_5$)), 1.79 (−CH$_2$C*H*$_2$C$_6$H$_{13}$), 1.5−1.1 (−C*H*$_2$−), 1.1−0.6 (−C*H*$_3$). IR (cm^{-1}): 3372 (br), 2956, 2923, 2853, 1627, 1517, 1483, 1456, 1377, 1305, 1232, 1179, 1122, 982, 824. GPC (UV-detector, 424 nm): M_n = 12 300 g/mol, M_w = 32 500 g/mol, polydispersity index (PDI) = 2.7.

Oligo(2,3-bis(2′-ethylhexyl)-5,7-bis(3-octylthiophen-2-yl)thieno[3,4-b]pyrazine) (6, *n* = 2, 3, 4, 5). Compound **3** (801 mg, 1.07 mmol) was dissolved in THF (10 mL). NBS (238 mg, 1.34 mmol) was added at 0 °C, in the absence of light. The mixture was stirred overnight while warming to room temperature. Diethyl ether (150 mL) was added, and the mixture was washed with water (3 × 50 mL) and saturated NaCl (2 × 50 mL). The organic phase was dried with MgSO$_4$, and the solvent was evaporated. The resulting monomer mixture was brought under an argon atmosphere. Ni(COD)$_2$ (555 mg, 2.02 mmol) and 2,2′-bipyridyl (315 mg, 2.02 mmol) were dissolved in toluene (20 mL) and stirred for 0.5 h at 80 °C. The Ni(COD)$_2$/bipyridyl mixture was added to the monomer mixture and stirred at 80 °C for 18 h. A 1:1:1 methanol/acetone/0.1 M HCl mixture (300 mL) was added, and the mixture was stirred for 1.5 h. The product was extracted with chloroform (2 × 150 mL), EDTA (disodium salt) (2 g) was added, and the mixture was stirred overnight. The mixture was washed with water (3 × 300 mL), concentrated, and precipitated in methanol (500 mL). The crude product mixture was filtered into a Soxhlet thimble and fractionated by Soxhlet extraction with methanol, acetone, hexane, dichloromethane, and chloroform. The hexane and dichloromethane extracts were separated by recycling GPC, yielding pure oligomers. Yields: dimer: 57 mg; trimer: 48 mg; tetramer: 33 mg; pentamer: 6 mg.

Dimer. ^{1}H NMR (400 MHz) δ (ppm): 7.36 (d, J = 5.2 Hz, 2p, Ar−*H*), 7.14 (s, 2p, Ar−*H*), 7.01 (d, J = 5.2 Hz, 2p, Ar−*H*), 2.97 (t, J = 2.7 Hz, 8p, −C*H*$_2$C$_7$H$_{15}$), 2.87 (m, 8p, −C*H*$_2$CH(C$_4$H$_9$)(C$_2$H$_5$)), 2.40−2.30 (m, 2p, −CH$_2$C*H*(C$_4$H$_9$)(C$_2$H$_5$)), 2.25−2.15 (m, 2p, −CH$_2$C*H*(C$_4$H$_9$)(C$_2$H$_5$)), 1.85−1.65 (m, 8p, −CH$_2$C*H*$_2$C$_6$H$_{13}$), 1.56−1.20 (m, 72p, −C*H*$_2$−), 1.04−0.84 (m, 36p, −C*H*$_3$). IR (cm^{-1}): 3079, 2956, 2922, 2872, 2853, 1516, 1487, 1457, 1377, 1235, 1182, 1122, 823, 813, 712. MALDI-TOF-MS *m*/*z* (intensity, %): 1494.61 (90), 1495.60 (100), 1496.60 (80), 1497.60 (50), 1498.60 (24), 1499.60 (10). GPC: 1 peak at 12.9 min.

Trimer. ^{1}H NMR (400 MHz) δ (ppm): 7.36 (d, J = 5.2 Hz, 2p, Ar−*H*), 7.14 (s, 4p, Ar−*H*), 7.01 (d, J = 5.2 Hz, 2p, Ar−*H*), 3.02−2.94 (m, 12p, −C*H*$_2$C$_7$H$_{15}$), 2.93−2.84 (m, 12p, −C*H*$_2$CH(C$_4$H$_9$)(C$_2$H$_5$)), 2.40−2.30 (m, 4p, −CH$_2$C*H*(C$_4$H$_9$)(C$_2$H$_5$)), 2.26−2.16 (m, 2p, −CH$_2$C*H*(C$_4$H$_9$)(C$_2$H$_5$)), 1.85−1.70 (m, 12p, −CH$_2$C*H*$_2$C$_6$H$_{13}$), 1.60−1.20 (m, 108p, −C*H*$_2$−), 1.05−0.80 (m, 54p, −C*H*$_3$). IR (cm^{-1}): 3079, 2956, 2922, 2871, 2853, 1517, 1485, 1457, 1377, 1350, 1239, 1181, 1122, 824, 813. MALDI-TOF-MS *m*/*z* (intensity, %): 2240.93 (55), 2241.93 (90), 2242.93 (100), 2243.92 (80), 2244.9 (50), 2245.92 (30), 2246.92 (15). GPC: 1 peak at 12.3 min.

Tetramer. ^{1}H NMR (400 MHz) δ (ppm): 7.36 (d, J = 5.2 Hz, 2p, Ar−*H*), 7.15 (m, 6p, Ar−*H*), 7.01 (d, J = 5.2 Hz, 2p, Ar−*H*), 3.04−2.84 (m, 32p, Ar−C*H*$_2$−), 2.42−2.30 (m, 6p, −CH$_2$C*H*(C$_4$H$_9$)(C$_2$H$_5$)), 2.26−2.16 (m, 2p, −CH$_2$C*H*(C$_4$H$_9$)(C$_2$H$_5$)), 1.87−1.70 (m, 16p, −CH$_2$C*H*$_2$C$_6$H$_{13}$), 1.60−1.20 (m, 144p, −C*H*$_2$−), 1.06−0.82 (m, 72p, −C*H*$_3$). IR (cm^{-1}): 3079, 2956, 2922, 2871, 2853, 1731, 1627, 1516, 1484, 1457, 1377, 1351, 1239, 1181, 1122, 824, 813. MALDI-TOF-MS *m*/*z* (intensity, %): 2987.58 (33), 2988.58 (70), 2989.6 (97), 2990.57 (100), 2991.57 (85), 2992.57 (60), 2993.57 (40), 2994.58 (25), 2995.57 (15). GPC: 1 peak at 11.9 min.

Pentamer. ^{1}H NMR (400 MHz) δ (ppm): 7.36 (d, J = 4.6 Hz, 2p, Ar−*H*), 7.15 (m, 8p, Ar−*H*), 7.01 (d, J = 5.2 Hz, 2p, Ar−*H*), 3.04−2.84 (m, 40p, Ar−C*H*$_2$−), 2.42−2.30 (m, 8p, −CH$_2$C*H*(C$_4$H$_9$)(C$_2$H$_5$)), 2.26−2.16 (m, 2p, −CH$_2$C*H*(C$_4$H$_9$)(C$_2$H$_5$)), 1.87−1.70 (m, 20p, −CH$_2$C*H*$_2$C$_6$H$_{13}$), 1.60−1.20 (m, 180p, −C*H*$_2$−), 1.06−0.82 (m, 90p, −C*H*$_3$). IR (cm^{-1}): 3077, 2955, 2922, 2871, 2853, 1516, 1483, 1457, 1377, 1350, 1239, 1180, 1134, 1122, 824, 813. MALDI-TOF-MS *m*/*z* (intensity, %): 3735.62 (80), 3736.60 (100), 3737.60 (98), 3738.49 (90), 3739.44 (70). GPC: 1 peak at 11.6 min.

Results and Discussion

Synthesis. The synthesis of the oligomers is outlined in Scheme 1. Condensation of compounds **1**[7] with **2** yielded the monomer **3**, which was (partially) brominated with NBS, yielding a mixture of mono- and dibrominated monomers (**4** and **5**). This mixture was then subjected to a nickel(0)-mediated Yamamoto coupling,[21] yielding a mixture of shorter oligomers **6** of various lengths. A rough separation of this mixture was accomplished by Soxhlet extraction. The different oligomers were further separated by recycling GPC. Recycling GPC is a preparative-scale GPC technique, in which the eluted products are fed back into the column, thereby virtually creating a GPC column of very high length, without having the problem of a very high pressure drop. During the run, the several oligomers can be collected, by temporarily switching the recycle valve to the collect position. This strategy yielded the monomer up to the pentamer (n = 1−5) in pure form as evidenced from GPC, MALDI-TOF mass spectrometry, and NMR. In the pentamer, the longest well-defined oligomer that was isolated in pure form, 15 aromatic units form the chain.

The corresponding polymer was also prepared by Yamamoto coupling from the dibrominated monomer. The polymer thus prepared had M_n =12 300 g/mol, M_w = 32 500 g/mol, resulting in a polydispersity of 2.7, as determined by GPC against polystyrene standards. The number average degree of polymerization of the polymer is $n \approx 16$, corresponding to ∼48 aromatic units.

Optical and Electrochemical Properties of the Neutral Oligomers. UV/vis absorption spectra of the oligomers, n = 1−5, are shown in Figure 1a. As expected, the absorption maxima (λ_{max}) and onsets (λ_{onset}) show a shift to higher wavelengths going from the monomer to the polymer. The extinction coefficients increase superlinearly with chain length. The optical band gaps (E_g^{opt}) estimated from the onsets of absorption are summarized in Table 1. The absorption spectrum of the polymer (Figure 1b) exhibits an extra shoulder at the low-energy side of the absorption spectrum. This is a clear signature of (partial) aggregation at room temperature in solution. At higher temperatures (above 40 °C) the polymer is molecularly dissolved. The onset of absorption for the polymer

SCHEME 1: Synthesis of the Oligomers and Polymer of 2,3-Bis(2′-ethylhexyl)-5,7-bis(3-octylthiophen-2-yl)thieno[3,4-b]pyrazine

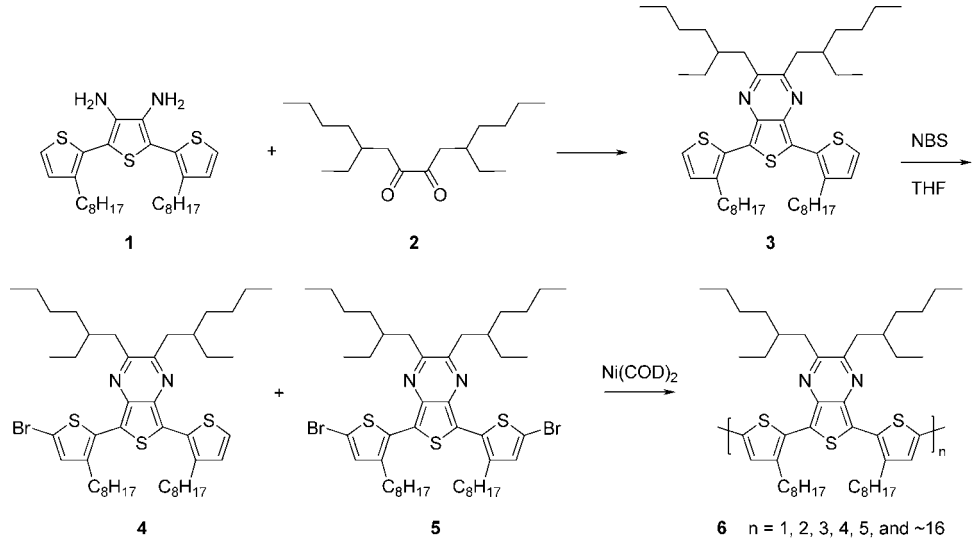

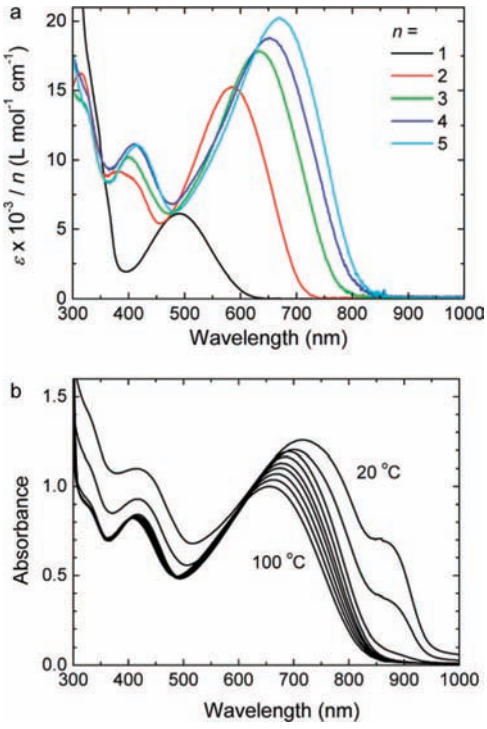

Figure 1. UV/vis absorption of (a) the monomer to the pentamer in toluene (the ordinate is the molar absorption coefficient (ε) divided by n, the number of monomeric units in the oligomer) at room temperature, and (b) the polymer at various temperatures in ODCB.

at 1.50 eV (when dissolved) and at 1.31 eV, (when aggregated), clearly identifies it as a small band gap conjugated polymer. In solution, the oligomers with $n > 1$ do not fluoresce, which indicates a high efficiency of internal conversion for these systems.

The redox behavior of the oligomers was investigated by cyclic voltammetry. The resulting voltammograms are shown in Figure 2. For the dimer to tetramer, two quasi-reversible oxidations are observed, which start to overlap in the pentamer. The reduction waves are irreversible, except for the monomer. The onset potentials of both oxidation (E_{ox}) and reduction (E_{red}) and the electrochemical band gap ($E_g^{cv} = E_{ox} - E_{red}$) are presented in Table 1.

The band gap of the oligomers decreases with increasing chain length (Table 1). The electrochemical band gap is slightly higher by 0.10 ± 0.05 eV than the optical band gap. Apart from experimental uncertainties, this difference reflects the fact that free ions are created in the electrochemical experiment rather than a neutral exciton. Apparently, this, combined with different solvation energies for the ions and the neutral molecule, causes E_g^{opt} and E_g^{cv} to be different. Both the dependence of the electrochemical and optical band gap on the inverse chain length and the dependence of the oxidation and reduction potentials on the inverse chain length ($1/n$) are shown in Figure 3.

In first approximation, both the oxidation and the reduction potentials follow a linear dependence with $1/n$. With increasing chain length the rise of the HOMO level (as reflected in the lowering of the oxidation potential) is responsible for most of the reduction of the band gap. The LUMO (reflected in the reduction potential) varies less. While a linear relation of the band gap with $1/n$ also seems valid for the band gap of the oligomers, the value for polymer deviates significantly from this straight line. It is well-known from literature that the optical band gaps of conjugated polymers can be fitted to the following equation:[22]

$$E(n) = E_\infty + (E_1 - E_\infty) \exp[-a(n-1)] \qquad (1)$$

Here, E_1 and E_∞ are the excitation energies for the monomer and the (infinitely long) polymer, n is the number of repeat units, and a is a parameter that describes how fast $E(n)$ saturates to E_∞. This empirical relation can be rationalized in terms of intrinsic length scales (electron−hole distances) and extrinsic length scales set by disorder.[23] If the optical band gaps for the oligomers are fitted to eq 1, a value of $E_\infty = 1.505$ eV is obtained, very close to the experimental value of 1.50 for the polymer. This fit is also shown in Figure 3. The value for a of 0.78 implies that the band gap stops decreasing between 7 and 10 repeat units (99% or 99.9% of the difference $E_1 - E_\infty$ has been reached, respectively). The data for the oligomers were also fitted according to the method by Kuhn[24] (Figure 4), where all N double bonds are regarded as identical, coupled oscillators. For the Kuhn model, only the double bonds in the conjugated chain are used, which, for the present oligomers, is given by $N = 6n$. This approach yields the same value of 1.5 eV for the optical band gap of the polymer (Figure 4).

TABLE 1: UV/Vis Absorption and PIA Data in Toluene and Onset of Redox Potentials (E_{ox} and E_{red}, vs Fc/Fc$^+$) in ODCB for the Oligomers and Polymer[a]

	λ_{max} (nm)	E_{max} (eV)	E_{ver}^{cal}(eV)	λ_{onset} (nm)	E_g^{opt} (eV)	E_{ox} (V)	E_{red} (V)	E_g^{cv}(eV)	$E_g^{cv} - E_g^{opt}$ (eV)	$T_n \leftarrow T_1$ (eV)	E_T^{cal} (eV)
monomer	493	2.52	2.67	605	2.05	0.20	−2.00	2.20	0.15	1.60[b]	0.97
dimer	587	2.11	2.30	706	1.76	−0.10	−1.92	1.82	0.06	1.40	0.90
trimer	632	1.96	2.11	768	1.61	−0.18	−1.92	1.74	0.13	1.32	0.88
tetramer	648	1.91	2.04	795	1.56	−0.21	−1.89	1.68	0.12	1.22	0.87
pentamer	669	1.85	2.01	809	1.53	−0.24	−1.87	1.63	0.10	1.20	0.87
polymer	671[c]	1.85[c]	n.d.	828[c]	1.50[c]	−0.26	−1.89	1.63	0.13	1.20[d]	n.d.

[a] $T_n \leftarrow T_1$ absorption in toluene. [b] Expected value based on eq 1. [c] In ODCB at 80 °C. [d] In chlorobenzene at 80 °C.

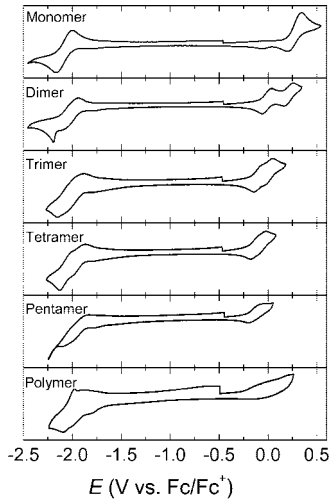

Figure 2. Cyclic voltammograms of the oligomers and the polymer recorded in ODCB.

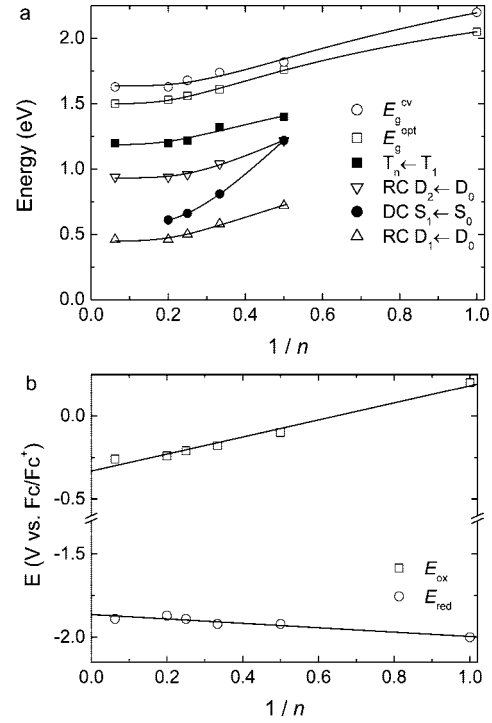

Figure 3. (a) Chain length dependence of energies for the optical E_g^{opt} and electrochemical band gap E_g^{cv}, the triplet $T_n \leftarrow T_1$ absorption, the radical cation (RC) absorptions ($D_1 \leftarrow D_0$ and $D_2 \leftarrow D_0$), and the dication (DC) absorption ($S_1 \leftarrow S_0$) versus reciprocal chain length ($1/n$). (b) Onsets of oxidation and reduction potentials vs $1/n$. Fits of the data (solid lines) in panel (a) are to eq 1, and those in panel (b) are to a linear relation with $1/n$.

Theoretical Results. The electronic and optical properties of the oligomers have also been characterized at a quantum-chemical level. The long alkyl side chains of the oligomers influence the solubility and the organization of the molecules in the solid state, but to a much lesser extent the electronic properties; we have thus substituted all of them by methyl groups to minimize the computational efforts. Since the correct determination of the actual torsion angles in solution is a rather challenging task, all molecular geometries were optimized by imposing the planarity of the systems. In view of the large size of the longest oligomers, we have optimized the ground-state geometry of the systems with the help of semiempirical Hartree−Fock techniques that generally provide the best compromise between computer times and accuracy of the geometric parameters. We have chosen here the semiempirical Hartree−Fock MNDO (modified neglect of differential overlap) method, as implemented in the AMPAC package,[25] which is known to provide geometric parameters in good agreement with experimental values for thiophene-based compounds;[26] in particular, MNDO yields a much better description of the C−C bond alternation compared to the widely used AM1 (Austin model 1) method.[26,27] The electronic structure was then calculated with the semiempirical Hartree−Fock INDO (intermediate neglect of differential overlap) method, as parametrized by Zerner and co-workers, and using the Ohno−Klopman potential.[28] INDO has been coupled to a single configuration interaction scheme including all $\pi \rightarrow \pi^*$ transitions to access the vertical transition energies between the ground and lowest excited states ($S_1 \leftarrow S_0$). This approach has been found to be the best compromise to depict the chain-length dependence of the optical properties of conjugated oligomers.[29] Note also that the combination of these two semiempirical techniques proves reliable to rationalize the optical properties of oligothiophenes.[30]

The vertical $S_1 \leftarrow S_0$ transition energies E_{ver}^{cal} calculated for all oligomers are shown in Figure 4 and are collected in Table 1. The experimental chain-size evolution is very well reproduced by the calculations. Moreover, we observe a fairly good quantitative agreement between the calculated transition energies and the experimental values of E_{max} that correspond to λ_{max} and that can be associated in first approximation to the vertical transition energies. Extrapolations to obtain the transition energies for the polymer were done using the Kuhn method[24] (solid line in Figure 4), which predicts the vertical transition for the polymer at $E_{ver}^{cal} = 1.93$ eV, while a slightly larger value of $E_{ver}^{cal} = 1.97$ eV is obtained with eq 1 (dashed line in Figure 4). These two values are in good agreement with the experimental value of $E_{max} = 1.85$ eV.

The $S_1 \leftarrow S_0$ transition of the monomer is mainly described by a HOMO $\rightarrow$ LUMO excitation. The corresponding shapes of the frontier molecular orbitals are shown in Figure 5. Despite the donor versus acceptor character of the two building blocks in the oligomers, the electronic density in the HOMO level is found to have a homogeneous distribution over the units while the LUMO has a more pronounced weight over the acceptor

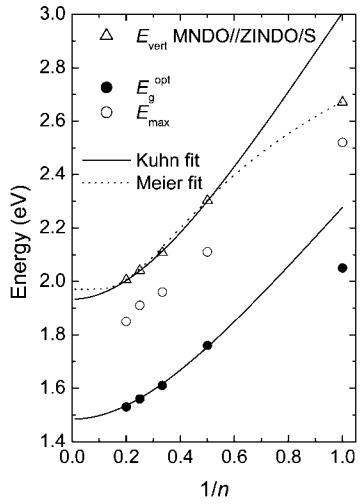

Figure 4. Calculated vertical transitions at the MNDO//ZINDO/S level of theory and experimental values for optical band gap and absorption maxima. Lines are extrapolation fits, following Kuhn[24] (solid line) and Meier[22] (eq 1, dotted line). n is the number of units in the oligomer and proportional to the number of double bonds along the conjugated chain ($N = 6n$).

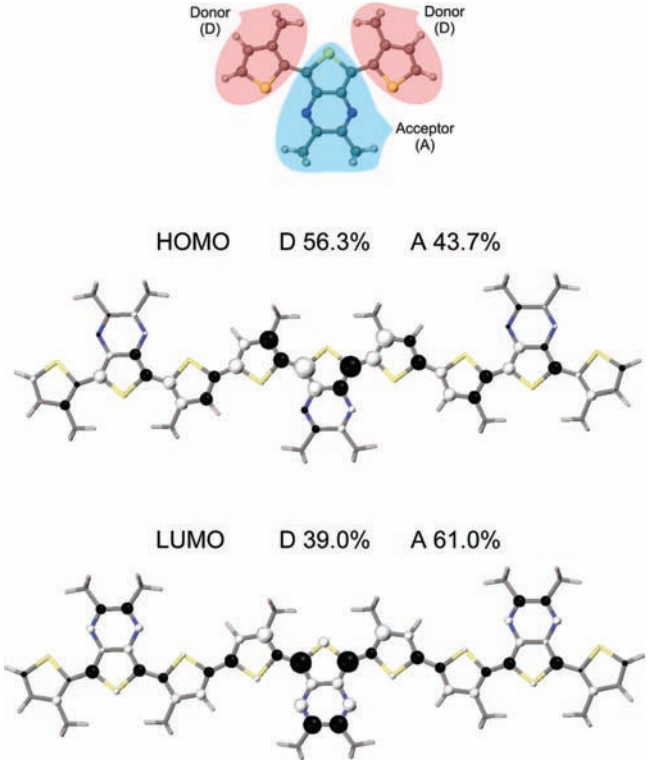

Figure 5. Shape of the frontier molecular orbitals and relative contributions of the donor (D) and acceptor (A) units; the color and size of the balls reflect the sign and amplitude of the linear combination of atomic orbitals (LCAO) coefficients.

parts.[31] This delocalization rationalizes the significant transition dipole moment (and hence oscillator strength) associated with the lowest optical transition. Another consequence is that a significant intramolecular charge transfer (~0.17e for the monomer) occurs upon promotion of an electron from the HOMO to the LUMO level.

Triplet Excited States. Triplet−triplet absorptions were investigated using near-steady-state PIA. Because formation of the triplet states of the oligomers by direct excitation to S_1, followed by intersystem crossing to T_1 was not successful, triplet

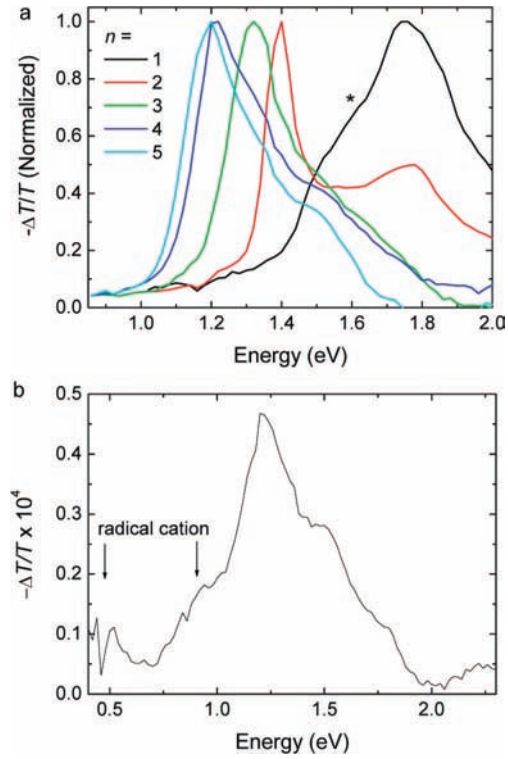

Figure 6. PIA spectra of (a) the oligomers recorded in toluene at room temperature and (b) the polymer in chlorobenzene at 80 °C. The expected location of the monomer triplet absorption is indicated with an asterisk in panel (a). In panel (b), the radical cation absorptions of the polymer are indicated with arrows.

states were populated by sensitization with a fullerene derivative (*N*-methylfulleropyrolidine, MP-C_{60}).[32] In this experiment, the fullerene is excited by the laser, and the triplet state of the fullerene is formed with a quantum yield of about unity. The triplet energy is then transferred from MP-C_{60} to the oligomer, yielding the triplet state of the oligomer. Mixtures of the oligomer (0.1 mM) and MP-C_{60} (0.4 mM) in toluene were excited by laser irradiation at 351 and 364 nm. The PIA spectra in toluene are shown in Figure 6. The PIA spectra of the oligomers exhibit a single strong absorption peak that shifts to lower energy with increasing n. In the case of the monomer, the triplet state of the monomer is not observed, but the typical PIA spectrum of MP-C_{60} with a peak at 1.78 and a shoulder at 1.52 eV is obtained.[32] Compared to a solution of pure MP-C_{60}, the triplet spectrum in the mixture is quenched by a factor of 15, indicating that the triplet state of the monomer is actually formed, yet not visible. Because of its poor solubility in toluene, the PIA spectrum of the polymer (375 μg/mL) was recorded in chlorobenzene, at 80 °C.

As can be seen, the $T_n \leftarrow T_1$ absorptions shift to lower energy as the length of the molecule increases. An overview of the $T_n \leftarrow T_1$ absorption maxima in toluene is given in Table 1. In the case of the polymer, also polaronic absorptions are visible in the PIA spectrum; this is due to the higher polarity of chlorobenzene compared to toluene. The more polar solvent stabilizes the charge separated state, where an electron is transferred from the polymer to MP-C_{60}.

The dependence of the $T_n \leftarrow T_1$ absorption maxima on the inverse chain length is depicted in Figure 3. Again, the absorption maxima for the dimer to the pentamer can be fitted to eq 1 to give $E_1 = 1.64$ eV, $E_\infty = 1.19$ eV, and $a = 0.73$. Careful inspection of the PIA spectrum of MP-C_{60} with the monomer leads to the observation of an extra shoulder in the

MP-C_{60} triplet absorption around 1.6 eV. This is exactly the region where the monomer triplet absorption would be expected, based on the fit discussed before. The extra shoulder is indicated in Figure 6 with an asterisk.

To estimate the energies of the T_1 state of the oligomers (E_T), quenching experiments were conducted. In these experiments, a triplet quencher with known triplet energy was added to the monomer/fullerene mixture. Quenching of the oligomer triplet indicates that the triplet energy of the oligomer is above the triplet energy of the quencher and vice versa. In this way, the T_1 triplet energies for the dimer to the pentamer were estimated to be between 0.93 eV (the triplet energy of bis(trihexylsiloxy)-silicon 2,3-naphthalocyanine)[33] and 1.14 eV (the triplet energy of rubrene).[34] The triplet level of the monomer was estimated to be around 1.14 eV (the triplet state of rubrene is only partially quenched by the monomer). In this way, the S_1-T_1 singlet−triplet splitting is estimated to be around 0.9 eV for the monomer, going to around 0.5 eV for the pentamer; the splitting for the dimer up to the tetramer is located somewhere in between. These values are roughly in correspondence with literature values of $\Delta E_{ST} \approx 0.7$ eV for most conjugated polymers.[35]

Theoretical support for these estimates for E_T was obtained by calculating the energies of the vertical $T_1 \leftarrow S_0$ transitions (E_T^{cal}) for the planar oligomers at the INDO/SCI level (Table 1). These vary from $E_T^{cal} = 0.97$ eV for the monomer to 0.87 eV for the pentamer and are, hence, slightly less than the experimental estimates ($0.93 < E_T \leq 1.14$ eV). In these calculations, the relaxation of the geometry in the triplet state, which will further reduce E_T^{cal}, was not taken into account. The overall small change in E_T compared to E_{ver}^{cal} with increasing chain length (n) suggests that the natural size of the triplet exciton is smaller than that of the singlet exciton.

Cations and Dications of the Oligomers. When applied in organic solar cells, photoexcited small band gap polymers donate an electron to an acceptor molecule, often a C_{60} derivative. The electron and hole are then separated, producing the photocurrent. To investigate the optical properties of the resulting oxidized species, chemical oxidation experiments and PIA experiments were performed.

Chemical oxidation of the oligomers can be accomplished by the addition of a strong oxidant. In this case, thianthrenium hexafluorophosphate[36] was added to a solution of the oligomers in dichloromethane in small aliquots. The UV/vis/NIR absorption spectra of the radical cations and of the dications that are produced in solution with increasing equivalents of thianthrenium were recorded. Results are shown in Figure 7. Chemical oxidation of the polymer was not performed, because of the poor solubility of the polymer in dichloromethane.

Upon oxidation of the monomer, bands corresponding to the radical cation or the dication of the monomer are absent (Figure 7a). Instead, the monomer radical cation is reactive and dimerizes to produce the dication of the dimer. As a result, the spectra of the monomer (Figure 7a) and the dimer (Figure 7b) both show a similar band at 1.22 eV. This observation is consistent with the fact that the first oxidation potential of monomer is higher than the second oxidation potential of the dimer (Figure 2). This dimerization is also visible in cyclic voltammetry. The first two scans for the monomer are depicted in Figure 8. In the second scan, the peaks of the dimer are clearly visible. In addition to the peak at 1.22 eV, the spectra of the oxidized monomer also show clear transitions at 1.92 and 2.13 eV. These are not related to the dimer dication, but, at present, we have no clear explanation for these features. Extrapolation of the determined $D_2 \leftarrow D_0$ transition energies for the other oligomers according to eq 1 (Figure 3) yields a value of 1.77 eV for the monomer. This value is much lower than 1.92 eV, and hence traces of monomer radical cation cannot satisfactorily explain the features at 1.92 and 2.13 eV.

For the dimer through the pentamer, the absorption band of the neutral oligomer decreases upon addition of the first equivalent thianthrenium hexafluorophosphate, while, at the same time, two new bands appear at lower energy. The new bands are attributed to the dipole-allowed $D_1 \leftarrow D_0$ and $D_2 \leftarrow D_0$ transitions of the doublet-state radical cation that, in first approximation, correspond to electron excitations from HOMO → SOMO (singly occupied molecular orbital) and SOMO → LUMO (see Figure 7f). For the pentamer, the low-energy $D_1 \leftarrow D_0$ band of the radical cation cannot be clearly observed, because it is located in the same region where the IR overtones of the solvent (dichloromethane) appear. Upon addition of a second equivalent of thianthrenium hexafluorophosphate, the radical cation bands decrease again, while an essentially single, new band with a vibronic feature at higher energy appears, located between the two bands of the radical cation. This band is attributed to the $S_1 \leftarrow S_0$ transition of the (singlet state) dication. In the case of the dimer, the high energy band of the radical cation overlaps with the band of the dication, and, with increasing conjugation length, the position of the dication band moves from the position close to the $D_2 \leftarrow D_0$ band for the dimer to that of the $D_1 \leftarrow D_0$ band for the pentamer (Figure 7). The positions of the radical cation and dication bands are collected in Table 2 and plotted versus $1/n$ in Figure 3. In Figure 3 it can be seen that dispersion of the dication transition with chain length is much stronger than that for the other transitions.

Photoinduced Electron Transfer in Solution from Oligomers to MP-C_{60}. In a PIA experiment with a mixture of the oligomers and MP-C_{60}, the nature of the formed excited-state depends on the polarity of the solvent. In apolar solvents, the triplet state energy of MP-C_{60} is transferred to the oligomer, giving rise to the triplet state of the oligomer (T_1), and the corresponding $T_n \leftarrow T_1$ absorption as shown in Figure 6. In polar solvents such as ODCB, however, the same experiment can result in an electron being transferred from the oligomer to the triplet state of MP-C_{60}, resulting in the radical cation of the oligomer and the radical anion of MP-C_{60}. The free energy for charge separation (ΔG_{CS}) in different solvents can be calculated by the Weller equation based on a continuum model:[37]

$$\Delta G_{CS} = e(E_{ox}(D) - E_{red}(A)) - E_{00} - \frac{e^2}{4\pi\varepsilon_0\varepsilon_s R_{cc}} - \frac{e^2}{8\pi\varepsilon_0}\left(\frac{1}{r^+} + \frac{1}{r^-}\right)\left(\frac{1}{\varepsilon_{ref}} - \frac{1}{\varepsilon_s}\right) \quad (2)$$

Here $E_{ox}(D)$ and $E_{red}(A)$ are the oxidation and reduction potentials of the donor (oligomer) and acceptor (MP-C_{60}, $E_{red}(A) = -1.20$ V vs Fc/Fc^+) in the reference solvent, respectively, E_{00} is the excited-state from which charge transfer takes place (1.50 eV for the triplet level of MP-C_{60}),[38] R_{cc} is the center-to-center distance of the positive and negative charges (set to infinity for intermolecular charge transfer), r^+ and r^- are the radii of the positive and negative ions, and ε_{ref} and ε_s are the relative permittivities of the reference solvent (used to measure oxidation and reduction potentials) and the solvent in which electron transfer is studied. r^- is calculated in literature to be 5.6 Å for C_{60}, based on the density of C_{60}.[38] r^+ can be estimated using a similar approach, using a density of 1.5, the value for unsubstituted terthiophene.[39] This calculation for the different oligomers yields the values given in Table 3. On the basis of

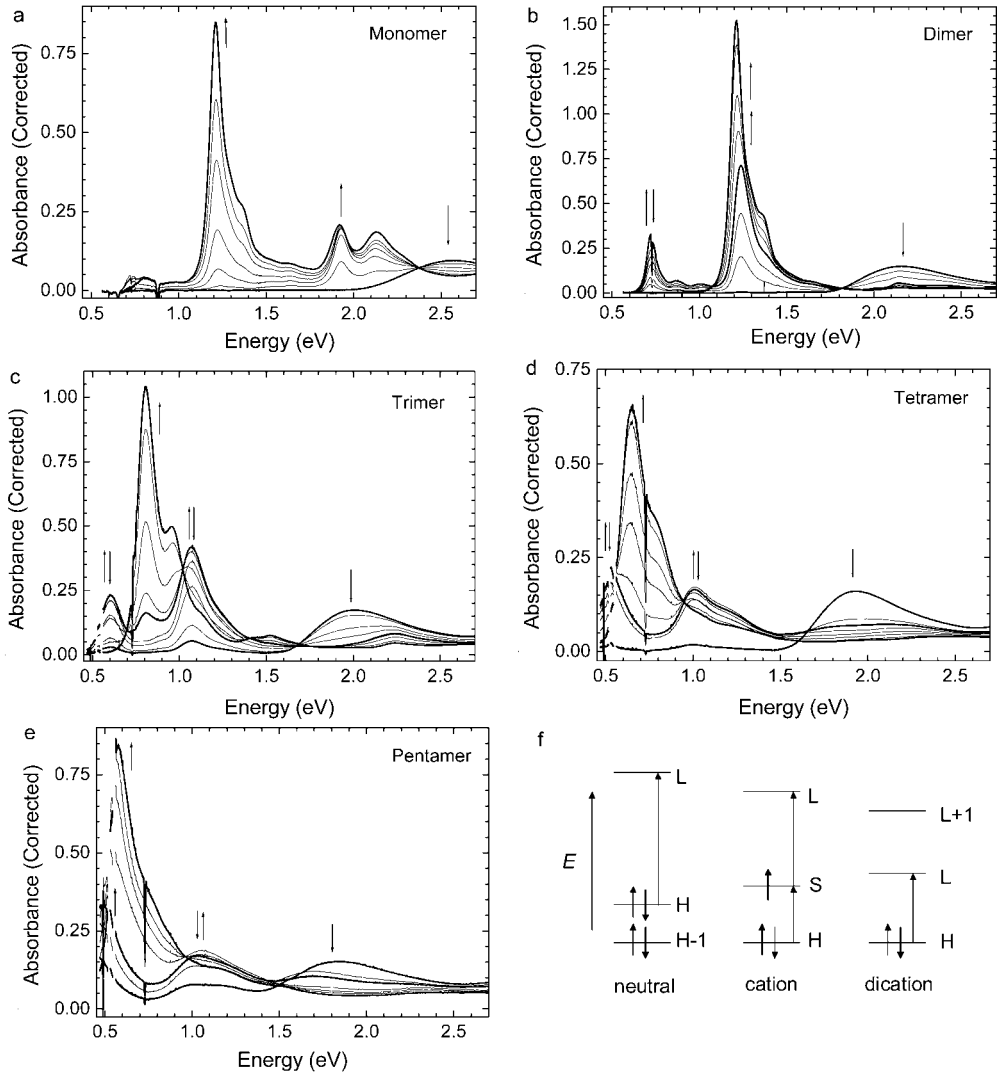

Figure 7. (a−e) Chemical oxidation of the oligomers in dichloromethane, by adding a solution of thianthrenium hexafluorophosphate. The appearance and disappearance of absorption bands is indicated with arrows. First, radical cations are produced, that are subsequently transformed into the dications. (f) Schematic orbital diagram for the main dipole-allowed transitions of the neutral oligomer, the cation, and the dication in a one-electron picture. (H = HOMO, S = SOMO, L = LUMO).

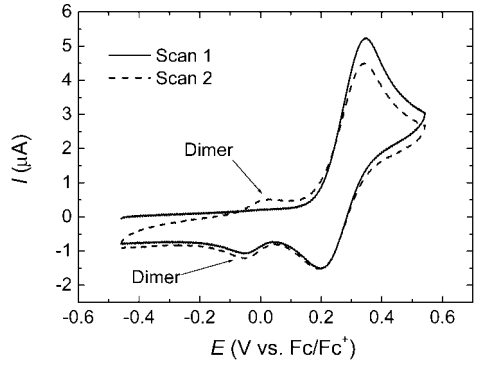

Figure 8. The first two scans in the cyclic voltammogram of the monomer; peaks belonging to the dimer are indicated.

these data we indeed expect triplet absorptions in toluene, but photoinduced electron transfer in ODCB.

The PIA spectra recorded of the oligomers in ODCB in the presence of MP-C_{60} are depicted in Figure 9. In order to prevent aggregation, the PIA spectrum of the polymer was recorded at 80 °C. As expected, the PIA spectra in ODCB show the two peaks of the radical cation of the oligomers ($n = 2-5$) and the polymer at low energies and a bleaching band at the absorption

TABLE 2: Absorption Maxima (eV) of the Principal Transitions of the Radical Cation (RC) and Dication (DC) of the Oligomers ($n = 2-5$) and the Polymer Determined from Chemical Oxidation and PIA Experiments

	chemical oxidation			PIA	
oligomer	RC $D_1 \leftarrow D_0$	RC $D_2 \leftarrow D_0$	DC $S_1 \leftarrow S_0$	RC $D_1 \leftarrow D_0$	RC $D_2 \leftarrow D_0$
dimer	0.72	1.22	1.22	0.72	1.22
trimer	0.60	1.07	0.81	0.58	1.04
tetramer	0.53	1.01	0.66	0.50	0.96
pentamer	0.46	1.04	0.61	0.46	0.94
polymer				0.46	0.94

energies of the neutral compounds. Absorption maxima of the oxidized oligomers determined by chemical oxidation and PIA in ODCB are given in Table 2; the data are also depicted in Figure 3. The radical anion of MP-C_{60}, which is expected to give a less intense transition at 1.24 eV,[32] is not clearly apparent from the spectra shown in Figure 9.

The values determined by PIA and chemical oxidation are in good agreement. The values determined in the PIA experiment are probably more reliable, because radical concentrations are much lower and reactions of these radicals are of less importance. Moreover, the low energy absorption bands of the longer oligomers are more visible in the PIA experiment,

TABLE 3: Free Energies for Charge Separation, Calculated Using Eq 2

			ΔG_{CS} (eV)	
oligomer	E^0_{ox} (ODCB) (V vs Fc/Fc^+)	r^+ (Å)	toluene	ODCB
monomer	0.27	4.3	0.92	−0.03
dimer	−0.01	5.4	0.53	−0.31
trimer	−0.10	6.2	0.39	−0.40
tetramer	−0.13	6.8	0.32	−0.43
pentamer	−0.16	7.4	0.27	−0.46

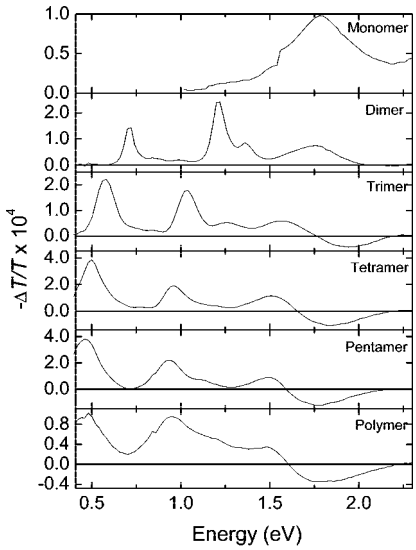

Figure 9. PIA spectra of the oligomers ($n = 1-5$) and the polymer recorded in ODCB in the presence of MP-C_{60}.

because of the lock-in detection. Going from pentamer to polymer, there is no decrease in transition energy anymore for both radical cation bands.

Conclusions

Well-defined lengthy oligomers, having up to 15 aromatic units, of a soluble poly(5,7-bis(thiophen-2-yl)thieno[3,4-b]pyrazine) were prepared. As expected, the optical band gap (E_g^{opt}) of the oligomers decreases with increasing chain length, and reaches a constant value of ~1.50 eV for seven repeating (trimeric) units. The electrochemical band gaps are slightly higher (0.10 ± 0.05 eV) than the optical band gaps. The redox potentials reveal that the major contribution (~75%) to the reduction of the optical band gap is the increase of the HOMO level with increasing chain length, rather than a reduction of the LUMO level (~25%). PIA experiments of a mixture of the oligomer with MP-C_{60} as sensitizer were used to generate the triplet state of the oligomers in toluene, via triplet-energy transfer. Going from monomer to polymer, the triplet ($T_n \leftarrow T_1$) absorption decreases in energy, showing the same trend as the $S_1 \leftarrow S_0$ absorption. The triplet state energies were estimated by quenching experiments, revealing that $\Delta E_{ST} \approx 0.9$ eV for the monomer, decreasing to around ~0.5 eV for the pentamer. These values are in agreement with previously reported values for conjugated systems.[35] In a more polar solvent, ODCB, electron transfer from the oligomer to the T_1 state of MP-C_{60} takes place rather than energy transfer, consistent with the estimated energy levels from a continuum model. The absorption bands determined for the oligomer radical cations produced in this way also shift to lower energy with increasing chain length. These are confirmed by chemical oxidation measurements that additionally provide insight into the absorption of the corresponding dications. The electronic and optical properties of the neutral oligomers were supported by quantum-chemical calculations. Inspection of the orbital coefficients for the HOMO and LUMO leads to the conclusion that both are roughly located on the same atoms (the LUMO is not solely localized on the acceptor units). This would give rise to a relatively large exchange energy and hence, to relatively large values for the singlet−triplet splitting, in agreement with experiment.

Acknowledgment. The research was supported by a TOP grant of the Chemical Sciences (CW) division of The Netherlands Organization for Scientific Research (NWO) and is part of the Joint Solar Programme (JSP). The JSP is cofinanced by the Foundation for Fundamental Research on Matter (FOM), Chemical Sciences of NWO, and the Foundation Shell Research. The joint collaboration is supported by the European Commission through the Human Potential Program Marie-Curie Research Training Network NANOMATCH (Grant No. MRTN-CT-2006-035884). The work in Mons is further supported by the Belgian National Fund for Scientific Research (FNRS). J.C. is a research fellow of FNRS. J.G. is a 'Ramón y Cajal' Research Fellow, financed by the Spanish Ministry for Education and Science.

References and Notes

(1) Padinger, F.; Rittberger, R. S.; Sariciftci., N. S. *Adv. Funct. Mater* **2003**, *13*, 85–88.
(2) Li, G.; Shrotriya, V.; Huang, J.; Yao, Y.; Moriarty, T.; Emery, K.; Yang, Y. *Nat. Mater.* **2005**, *4*, 864–868.
(3) Ma, W. L.; Yang, C. Y.; Gong, X.; Lee, K.; Heeger, A. J. *Adv. Funct. Mater.* **2005**, *15*, 1617–1622.
(4) Winder, C.; Sariciftci, N. S. *J. Mater. Chem.* **2004**, *14*, 1077–1086.
(5) Kitamura, C.; Tanaka, S.; Yamashita, Y. *Chem. Mater.* **1996**, *8*, 570–578.
(6) Wang, X. J.; Perzon, E.; Delgado, J. L.; de la Cruz, P.; Zhang, F. L.; Langa, F.; Andersson, M.; Inganas, O. *Appl. Phys. Lett.* **2004**, *85*, 5081–5083.
(7) Campos, L. M.; Tontcheva, A.; Gunes, S.; Sonmez, G.; Neugebauer, H.; Sariciftci, N. S.; Wudl, F. *Chem. Mater.* **2005**, *17*, 4031–4033.
(8) Muhlbacher, D.; Scharber, M.; Morana, M.; Zhu, Z. G.; Waller, D.; Gaudiana, R.; Brabec, C. *Adv. Mater.* **2006**, *18*, 2884–2889.
(9) Zhang, F.; Mammo, W.; Andersson, L. M.; Admassie, S.; Andersson, M. R.; Inganas, O. *Adv. Mater.* **2006**, *18*, 2169–2173.
(10) Wienk, M. M.; Turbiez, M. G. R.; Struijk, M. P.; Fonrodona, M.; Janssen, R. A. J. *Appl. Phys. Lett.* **2006**, *88*, 153511.
(11) Wienk, M. M.; Struijk, M. P.; Janssen, R. A. J. *Chem. Phys. Lett.* **2006**, *422*, 488–491.
(12) Perzon, E.; Zhang, F. L.; Andersson, M.; Mammo, W.; Inganas, O.; Andersson, M. R. *Adv. Mater.* **2007**, *19*, 3308–3311.
(13) Zhu, Y.; Champion, R. D.; Jenekhe, S. A. *Macromolecules* **2006**, *39*, 8712–8719.
(14) Bundgaard, E.; Krebs, F. C. *Sol. Energy Mater.* **2007**, *91*, 954–985.
(15) Peet, J.; Kim, J. Y.; Coates, N. E.; Ma, W. L.; Moses, D.; Heeger, A. J.; Bazan, G. C. *Nat. Mater.* **2007**, *6*, 497–500.
(16) Roncali, J. *Chem. Rev.* **1997**, *97*, 173–205.
(17) Van Mullekom, H.A. M.; Vekemans, J. A. J. M.; Havinga, E. E.; Meijer, E. W. *Mater. Sci. Eng., R* **2001**, *32*, 1–40.
(18) Van Mullekom, H. A. M.; Vekemans, J. A. J. M.; Meijer, E. W. *Chem.—Eur. J.* **1998**, *4*, 1235–1243.
(19) Ozen, A. S.; Atilgan, C.; Sonmez, G. *J. Phys. Chem. C* **2007**, *111*, 16362–16371.
(20) Salzner, U.; Karalti, O.; Durdagi, S. *J. Mol. Model.* **2006**, *12*, 687–701.
(21) Yamamoto, T.; Morita, A.; Miyazaki, Y.; Maruyama, T.; Wakayama, H.; Zhou, Z.; Nakamura, Y.; Kanbara, T.; Sasaki, S.; Kubota, K. *Macromolecules* **1992**, *25*, 1214–1223.
(22) Meier, H.; Stalmach, U.; Kolshorn, H. *Acta Polym.* **1997**, *48*, 379–384.
(23) Rissler, J. *Chem. Phys. Lett.* **2004**, *395*, 92–96.
(24) Kuhn, W. *Helv. Chim. Acta* **1948**, *31*, 1780–1799.
(25) *AMPAC 6.55*, Semichem: Shawnee, KS, 1997.
(26) Adant, C.; Beljonne, D.; Brédas, J. L. *J. Chem. Phys.* **1994**, *101*, 8048–8054.
(27) Cornil, J.; Beljonne, D.; Brédas, J. L. *J. Chem. Phys.* **1995**, *103*, 842–849.

(28) Ridley, J.; Zerner, M. *Theor. Chim. Acta* **1973**, *32*, 111–134.
(29) Gierschner, J.; Cornil, J.; Egelhaaf, H. J. *Adv. Mater.* **2007**, *19*, 173–191.
(30) Beljonne, D.; Cornil, J.; Friend, R. H.; Janssen, R. A. J.; Brédas, J. L. *J. Am. Chem. Soc.* **1996**, *118*, 6453–6461.
(31) A similar pattern is obtained at the density functional theory (DFT) level, using the widely used B3LYP functional and a 6-31G* basis set, thus demonstrating the reliability of the semi-empirical approaches.
(32) Van Hal, P. A.; Beckers, E. H. A.; Peeters, E.; Apperloo, J. J.; Janssen, R. A. J. *Chem. Phys. Lett.* **2000**, *328*, 403–408.
(33) Firey, P. A.; Ford, W. E.; Sounik, J. R.; Kenney, M. E.; Rodgers, M. A. J. *J. Am. Chem. Soc.* **1988**, *110*, 7626–7630.
(34) Herkstroeter, W. G.; Merkel, P. B. *J. Photochem.* **1981**, *16*, 331–341.
(35) Kohler, A.; Beljonne, D. *Adv. Funct. Mater.* **2004**, *14*, 11–18.
(36) Shine, H. J.; Zhao, B. J.; Marx, J. N.; Ould-Ely, T.; Whitmire, K. H. *J. Org. Chem.* **2004**, *69*, 9255–9261.
(37) Weller, A. *Z. Phys. Chem. Neue Folge* **1982**, *133*, 93–98.
(38) Williams, R. M.; Zwier, J. M.; Verhoeven, J. W. *J. Am. Chem. Soc.* **1995**, *117*, 4093–4099.
(39) Van Bolhuis, F.; Wynberg, H.; Havinga, E. E.; Meijer, E. W.; Staring, E. G. J. *Synth. Met.* **1989**, *30*, 381–389.

JP805817C